Applied Thermal Engineering 171 (2020) 115073

Contents lists available at ScienceDirect

Applied Thermal Engineering

journal homepage: www.elsevier.com/locate/apthermeng

Numerical study on thermohydraulic behavior in compensation chamber of a loop heat pipe with flat evaporator

Zikang Zhang, Hao Zhang, Xiaotian Lai, Zhichun Liu, Wei Liu*

School of Energy and Power Engineering, Huazhong University of Science and Technology, Wuhan 430074, China

HIGHLIGHTS

- Subcooled flow boiling happens inside compensation chamber due to high heat leak.
- Formation of vapor phase in compensation chamber causes temperature fluctuation.
- Uneven vapor distribution and turbulence intensification convert flow structure.
- Low mass flowrate and high heat leak raise subcooled flow boiling intensity.
- Environmental convection does slight effect on heat and mass transfer process.

ARTICLE INFO

Keywords:
Loop heat pipe
Compensation chamber
Volume of fluid method
Subcooled flow boiling
Temperature fluctuation

ABSTRACT

Numerical simulations have been conducted extensively in the researches of loop heat pipe during recent years for capturing the precise mechanism. In this study, a three-dimensional computational fluid dynamic model of compensation chamber in pump-assisted loop heat pipe was developed for investigating the thermohydraulic mechanism systematically. In order to explain the temperature fluctuation inside compensation chamber while high heat leak was considered, numerical simulation was implemented by adopting the volume of fluid method. The characteristic of heat transfer was determined by the vapor distribution and heat flux variation. Simulation results indicated the existence of subcooled flow boiling inside compensation chamber. Additionally, bubbles mainly got formed on wick surface, and a flow structure transform was found due to the uneven vapor distribution and turbulence intensification. Decreasing in mass flowrate or increasing in heat leak led to an augmentation of vapor volume and nucleation site density. However, environmental convection showed slight influence on heat and mass transfer.

1. Introduction

Loop heat pipe (LHP) is a two-phase heat-transfer device which transports high intensity heat flux by the vaporization and condensation of working fluid [1]. With its reliability and efficiency in the thermal control systems such as thermal management of satellites [2] and cooling systems of electronics [3–5], LHP has been investigated systematically by more and more researchers and companies. Compared with conventional heat pipes, LHP allows more flexible location of evaporator/condenser and configuration design of evaporator, which further extends its application.

LHP consists of an evaporator where phase change takes place, a condenser to dissipate heat load, a vapor and liquid line to transport working medium. On account of the existence of porous media and phase change, LHP has complex heat and mass transfer mechanism and needs to be understood for further improvement of the system design. During the recent decades, numerous experimental and numerical investigations have been conducted to reveal the operating mechanism of LHP. Singh et al. [6] investigated the effect of wick structures with different physical properties on heat transfer characteristics. Esarte et al. [7] adopted the 3D selective laser melting printing technology to fabricate the wick. The effect of fluid charge ratio and ambient temperature was studied as well.

Generally, researches on the modeling of LHP can be divided into two categories. One focuses on the loop operation by constructing thermal resistance network and divides the circuit into several computational domains and nodes. Siedel et al. [8,9] developed a steady-state analytical model to investigate the thermohydraulic behavior of a flat LHP. Their simulation presented the major influence of evaporation coefficient and wick conductivity on LHP performance. Vlassov et al.

* Corresponding author.
E-mail address: w_liu@hust.edu.cn (W. Liu).

https://doi.org/10.1016/j.applthermaleng.2020.115073
Received 6 September 2019; Received in revised form 7 February 2020; Accepted 11 February 2020
Available online 11 February 2020
1359-4311/

Nomenclature

A_w	heat transfer surface area [m^2]
c	specific heat [J kg^{-1} K^{-1}]
E	specific energy [J kg^{-1}]
F_{vol}	source term of the volume force [kg m^{-2} s^{-2}]
g	gravity [N kg^{-1}]
h_{fg}	latent heat of vaporization [J kg^{-1}]
h_c	convective heat transfer coefficient [W m^{-2} K^{-1}]
k	thermal conductivity [W m^{-1} K^{-1}]
$\boldsymbol{n}$	surface normal [m^{-1}]
p	pressure [Pa]
Q	surface heat flux [W]
$S_{m,l}$	liquid source term [kg m^{-3} s^{-1}]
$S_{m,v}$	vapor source term [kg m^{-3} s^{-1}]
S_q	energy source term [W m^{-3}]
t	time [s]
T	temperature [K]
$\boldsymbol{u}$	velocity vector [m s^{-1}]

Greek symbols

α	volume fraction
ε	porosity [%]
κ	interphase curvature [m^{-1}]
λ	relaxation factor [s^{-1}]
μ	dynamic viscosity [N s m^{-2}]
ρ	density [kg m^{-3}]
σ	coefficient of surface tension [N m^{-1}]

Subscripts

cc	compensation chamber
e	evaporator shell outer surface
eff	effective
es	evaporator shell internal surface
i	adiabatic
in	inlet
l	liquid
out	outlet
sat	saturation
v	vapor
w	wick surface
wick	porous media

[10] provided a mathematical model of a LHP, tracking the two-phase interface and distribution of different phase in the circulation. Bai et al. [11,12] constructed a LHP with a two-layer compound wick and modelled it on energy conservation law. Results indicated an improvement by using this new wick than conventional single-layer wick. Maydanik et al. [13] conducted the start-up regime simulation under different heat loads and structural materials of the evaporator. Masahito et al. [14] studied the transient response and heat load distribution with a 1-D transient mathematical model. Numerical simulation showed a temperature overshoot caused by the overestimation of heat leak. Changwoo et al. [15] numerically investigated the operational characteristic of a mechanical-capillary-driven two-phase LHP and results showed good agreement with the experiment.

The other subgroup concentrates on heat and mass transfer in evaporator by using CFD analysis. Ji Li et al. [16] constructed a practical quasi 3-D numerical model. They conjugated heat transfer problem with mass transfer in a fully saturated wicking structure. Ghajar et al. [17,18] provided a numerical investigation on a novel micro loop heat pipe (MLHP) by hybridizing an alternating direction implicit CFD code and relevant thermodynamic equations. The optimized geometric feature was found by such method to improve the design of the MLHP. Maydanik et al. [19] presented a 3-D mathematical model combining all the main structural elements of the evaporator. A drying condition in the wick under high heat load was considered as well. Zhao et al. [20,21] investigated the heat conduction process inside a 3-D porous media in LHP by using a lattice Boltzmann model and proved that it was applicable to predict the performance of an actual structure. Masahito et al. [22] developed a three-dimensional pore network model considering pore size dispersion to investigate the heat-transfer characteristics of a LHP. They concluded that the optimal shape could be determined by varying the three-phase contact line. Pozhilov et al. [23] constructed a mathematical model to simulate the LHP evaporator in TacSat-4 satellite. Reynolds-averaged Navier-Stokes equation and Darcy's law were contained in the numerical simulation and a non-uniform heat load distribution on the evaporator was revealed.

Researches above can annotate the physical mechanism for LHP in some ways. As for the CC which acted as a container for the excess working fluid, those papers considered that it operated with single-phase heat transfer and ignored the phase change that might exist for simplification. Experimental studies indicated that at low or medium heat load, the heat leak from wick and evaporator shell to compensation chamber was too high to be compensated by the subcooled fluid with low mass flowrate, which then caused saturated boiling. These would lead to the temperature fluctuation and even damage the stable operation of the system [24–27]. Maydanik et al. [28] developed a 3-D numerical model to reveal the heat and mass transfer in CC by using EFDLab. Anand et al. [29] experimentally studied the miniature LHP by visualizing the working fluid in CC. Their results demonstrated that there was an explosive nucleation due to high heat leak, causing a rapid rise in operating temperature and the consequential system failure. Spinato et al. [30] studied the liquid/vapor interface dynamics by using time-strip image processing technique and found out that the oscillating flow was produced by nucleation and bubble expansion. With the assistance of the pump, the phase change could be restrained and only occurred under high heat flux, the temperature fluctuation amplitude was reduced as well. All of these improved the operating performance to some extent [31].

Based on the former experimental studies about the pump-assisted loop heat pipe [31–33], this paper presents a three-dimensional CFD model to obtain specific heat exchange and vapor distribution in the CC. The multiphase flow model is the volume of fluid (VOF) method [34] which has been widely employed to investigate the subcooled flow boiling in micro-channels [35,36]. Also it has been used to visualize the boiling and condensation in conventional heat pipe [37] and miniature oscillating heat pipe [38]. The internal heat and mass transfer mechanism is revealed by calculating the distribution of bubbles and nucleation sites, and the impact on the flow structure is evaluated by altering mass flowrate, heat leak distribution and environmental convection. Simulation results reveal that the flow inside CC is considered to be subcooled flow boiling. Mass flowrate and heat leak distribution affect the subcooled flow boiling intensity greatly. The present study can get better understanding on temperature fluctuation and it also provides a theoretical basis for further investigation on evaporator simulation.

2. Mathematical model

2.1. Continuity equation for VOF model

By using the mass conservation law, the sum of liquid and vapor

phase volume fractions satisfies the following equation,

$$\alpha_l + \alpha_v = 1. \tag{1}$$

For different phase, the continuity equations can be written as

$$\frac{\partial \alpha_l}{\partial t} + \nabla\cdot(\mathbf{u}_l\alpha_l) = \frac{S_{m,l}}{\rho_l}, \tag{2}$$

$$\frac{\partial \alpha_v}{\partial t} + \nabla\cdot(\mathbf{u}_v\alpha_v) = \frac{S_{m,v}}{\rho_v}. \tag{3}$$

The liquid and vapor source terms about mass transfer during condensation and evaporation are expressed by $S_{m,l}$ and $S_{m,v}$, and the relation is $-S_{m,l} = S_{m,v}$. The liquid is the primary phase while the vapor is the secondary phase. By comparing the local temperature with saturation temperature, the boiling and condensation condition can be determined and the source terms through two-phase interface are defined as

$$S_{m,v} = \lambda\alpha_l\rho_l\frac{T_l - T_{sat}}{T_{sat}} \quad T_l \geqslant T_{sat}, \tag{4}$$

$$S_{m,l} = \lambda\alpha_v\rho_v\frac{T_v - T_{sat}}{T_{sat}} \quad T_v \leqslant T_{sat}, \tag{5}$$

where λ is the relaxation factor, T_{sat} is the saturation temperature of the working medium.

For the mixture of liquid and vapor, its physical parameters such as density, thermal conductivity, dynamic viscosity, etc. can be deducted by the volume-fraction-average,

$$\rho = \alpha_l\rho_l + \alpha_v\rho_v. \tag{6}$$

2.2. Momentum equation for VOF model

Taking gravitation, friction, pressure, and surface tension into consideration, the momentum equation can be written as

$$\frac{\partial\rho\mathbf{u}}{\partial t} + \nabla\cdot(\rho\mathbf{u}\mathbf{u}^T) = -\nabla p + \nabla\cdot\left[\mu(\nabla\mathbf{u} + \nabla\mathbf{u}^T) - \frac{2}{3}\mu(\nabla\cdot\mathbf{u})\mathbf{I}\right] + \rho\mathbf{g} + F_{vol}, \tag{7}$$

where $\boldsymbol{I}$ is the unit tensor. The F_{vol} deduced by the continuum surface force (CSF) model [39] can be expressed as

$$F_{vol} = \sigma\frac{\alpha_l\rho_l\kappa_v\nabla\alpha_v + \alpha_v\rho_v\kappa_l\nabla\alpha_l}{0.5(\rho_l + \rho_v)}, \tag{8}$$

where σ represents surface tension coefficient between liquid and vapor, κ is the interphase curvature and can be written as

$$\kappa = \nabla\cdot\frac{\mathbf{n}}{|\mathbf{n}|}, \tag{9}$$

$$\mathbf{n} = \nabla\alpha_k. \tag{10}$$

2.3. Energy equation for VOF model

The energy equation can be written as

$$\frac{\partial}{\partial t}(\rho E) + \nabla\cdot[\mathbf{u}(\rho E + p)] = \nabla\cdot[k\nabla T] + S_q. \tag{11}$$

The source term on account of the heat transfer from phase change is represented as S_q, and it observes

$$S_q = -h_{fg}S_{m,l} = h_{fg}S_{m,v}. \tag{12}$$

The VOF model treats the energy E as a mass-averaged variable,

$$E = \frac{\alpha_l\rho_l E_l + \alpha_v\rho_v E_v}{\alpha_l\rho_l + \alpha_v\rho_v}, \tag{13}$$

$$E_l = c_{v,l}(T - T_{sat}), \tag{14}$$

$$E_v = c_{v,v}(T - T_{sat}), \tag{15}$$

where h_{fg} is the latent heat of vaporization, c_v is the specific heat of each phase.

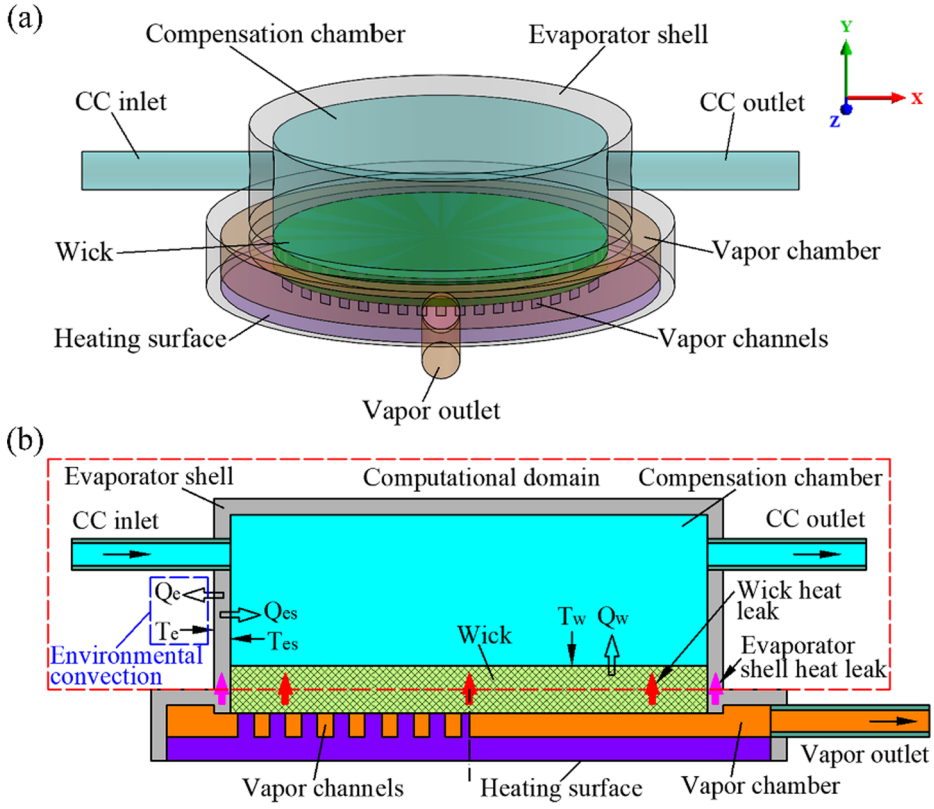

Fig. 1. Geometrical model of evaporator: (a) schematic of the flat disk evaporator; (b) the rotated sectional view of evaporator.

2.4. Model geometry

The evaporator is one of the most critical components in pump-assisted LHP which consists of compensation chamber, wick, and evaporation chamber. Fig. 1(a) describes the evaporator structure in this paper. Subcooled liquid from pump enters the CC through CC inlet. Then the bulk of fluid absorbs heat leak from evaporator shell and wick before flowing out through CC outlet. Only a small fraction of fluid can get into the vapor chamber through wick driven by capillary force. During boiling process, the working fluid can take away most of the heat load from heating surface, and the generated vapor is then ejected through vapor channels into vapor outlet. Two sets of condensers are designed to cool down two separate flow from the evaporator. Before entering the pump, two streams of subcooled liquid are joined together by using an ejector. The schematic of the pump-assisted LHP is described in Ref. [32].

Due to the location of CC and complex coupling between each part of the LHP, the high heat leak may cause phase change in CC and result in unstable operation. By applying pump-assisted configuration, the saturated boiling can be weakened into subcooled flow boiling under the effect of large mass flowrate. However, such subcooled flow boiling still causes temperature fluctuation. Therefore, a three-dimensional numerical model is developed by Fluent 16.0 and the subcooled flow boiling is solved by using the VOF method. In order to get detail flow behavior in CC, meanwhile take notice of the huge discrepancy of mass flowrate between CC outlet and vapor chamber outlet, only CC side which is half of the evaporator is considered so as to reduce the computational consumption. Most of the peculiarities structure and geometry configuration is taken into account. Wick considers half of the actual one. Fig. 1(b) illustrates the computational domain with a red dash line and Table 1 provides the main parameters of the model.

2.5. Definite condition

The use of the VOF method needs the simulation to be conducted in a transient way, which may increase the calculation time. For solving this problem, the following assumptions are made for the model.

(1) Thermophysical properties of the fluid are considered to be constant.
(2) Continuous medium hypothesis is satisfied.
(3) The flow inside the wick is neglected.
(4) Fluid is incompressible.

The effective thermal conductivity and other thermophysical properties of the wick are determined by a weighted average method and can be written as

$$k_{eff} = \varepsilon k_l + (1 - \varepsilon) k_{wick}, \tag{16}$$

$$\rho_{eff} = \varepsilon \rho_l + (1 - \varepsilon) \rho_{wick}, \tag{17}$$

$$c_{p,eff} = \varepsilon c_{p,l} + (1 - \varepsilon) c_{p,wick}, \tag{18}$$

where ε is the porosity of the wick. k, ρ, c_p represent the thermal conductivity, density and specific heat capacity respectively.

During the calculation, time-step shall be modified to satisfy an appropriate calculation speed without lowering the precision. An alternative method named variable time stepping is applied to automatically alter the time-step by determining a suitable Courant number and the computational consumption can be reduced. The SST k-w turbulent model and pressure-based solver are chosen in the model. Momentum and energy discretization method are QUICK method. Pressure-Implicit with Splitting of Operators (PISO) coupling is adopted as the pressure–velocity coupling method. PRESTO and Geometric Reconstruction Scheme are utilized for the interpolation scheme of the pressure and volume fraction. The specific interface of the bubble can be got by the Piecewise Linear Interface Calculation (PLIC). A mesh sensitivity study of the grid-independence is achieved when the number of grid reaches 1248394. The convergence limitation is set as the residuals lowering than 10^{-4}.

Velocity inlet boundary and pressure outlet boundary are applied to the CC inlet and outlet. Different heat flux boundary conditions are used on two zones to simulate different heat leaks. One is on the bottom of the wick and the other is on the bottom of the evaporator shell. The distribution of heat leaks is described in Fig. 1(b). All interfaces inside the model are set as coupled wall and imposed as non-slip boundary condition. Heat transfer with the environment is not considered unless explicit illustration. First, the initiate data file is solved without applying phase change source terms, under this situation fluid near the wick enters an overheating state. Next, the transient calculation is conducted with source terms added by UDFs, and then the overheated liquid will transfer into vapor. By this way, the development velocity of flow field can be quickened and the computing speed can be increased.

3. Results and discussion

3.1. Preliminary study of heat and mass transfer in CC

A series of numerical calculation cases listed in Table 2 are performed to investigate the influence of mass flowrate, heat leak distribution and environmental convection. Boundary conditions are set as follow by referring to the Refs. [8,40]. The saturation temperature is 30 °C and the contact angle of bubbles on interface is 90°. This section suggests case 2 as a representative sample to get a more precise understanding of the hydrodynamic behaviors. Heat load in the heating zone is set to 100 W. The total heat leak accounts for 12% of the heat load and the ratio of heat leaks between wick and evaporator shell is 2:1, that means heat leak is 8 W from wick and 4 W from evaporator shell. The transient calculation consumes around 10 s from initial state to a steady state.

Table 1
Main parameters of the computational domain.

Components		Dimensions
Evaporator shell	Diameter I/O	35/41 mm
	Height I/O	10/13 mm
	Material	Stainless steel
	Working fluid	Methanol
CC inlet/outlet line	Inner diameter of the inlet/outlet	4 mm
	Length of the inlet/outlet	20 mm
Wick	Diameter	35 mm
	Thickness	1.5 mm
	Porosity	69%
	Material	Nickel

Table 2
Boundary conditions for simulation.

Simulation case no.	CC inlet temperature (K)	Mass flowrate (g/s)	Wick heat leak (W)	Evaporator shell heat leak (W)	Environmental heat loss
1	25	3.75	8	4	Not applied
2	25	7.5	8	4	
3	25	11.25	8	4	
4	20	7.5	8	4	
5	20	7.5	12	6	
6	20	7.5	6	12	
7	20	7.5	12	6	Applied

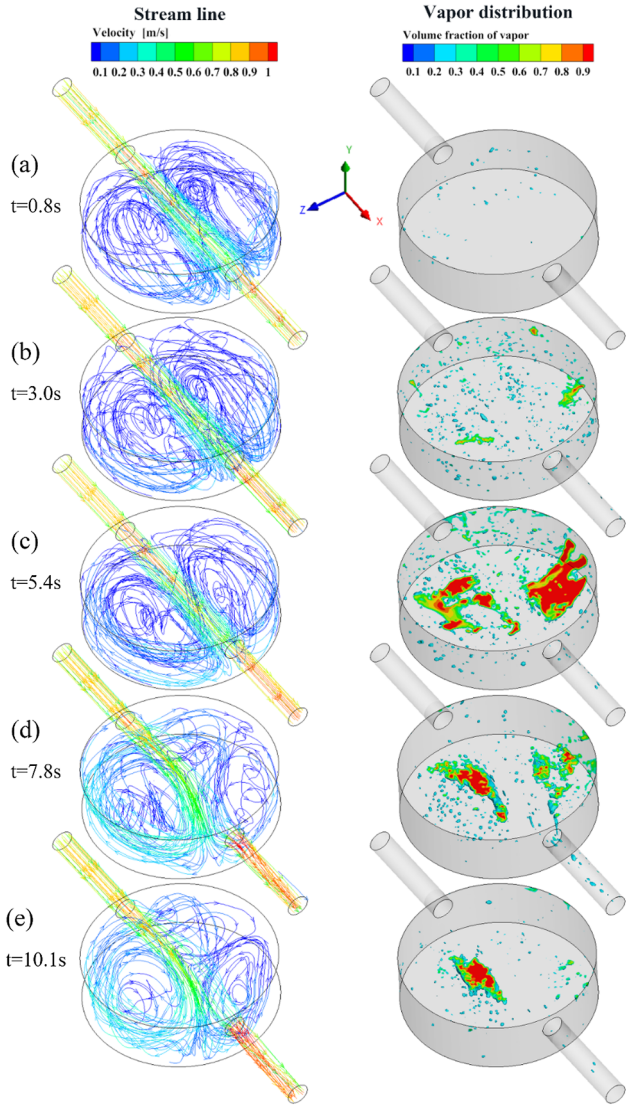

Fig. 2. Streamline and vapor distribution in compensation chamber: (a) t = 0.8 s; (b) t = 3.0 s; (c) t = 5.4 s; (d) t = 7.8 s; (e) t = 10.1 s.

Fig. 2 shows the streamline of fluid and vapor distribution in CC at 5 discrete moments. The bubble is described by ignoring vapor volume fraction below 0.25. The appearance of bubbles indicates that under the boundary conditions above, there is a phase change happened inside CC which can be characterized as subcooled flow boiling. In the first 5 s, two symmetrical vortices are developed originated from the structural constraints, and bubbles accumulate in the upper part of the chamber after the generation on wick surface. At the last 5 s, vapor starts to flow out with the main flow, and CC outlet turns to gas–liquid two-phase flow, which leads to a temperature fluctuation. In addition, there is an obvious variation in streamline, the vortex on one side dominates and two or more small vortices form on the other side instead of a symmetrical vortex. The generation of asymmetrical vortices is caused by two factors. One factor is the discrepancy of vapor distribution. From Fig. 2, it is clearly to see that bubbles on the right side flow out at 7.8 s, causing a large offset on streamline, and the symmetrical vortices shift into an asymmetrical structure. The other factor is the increase in turbulence intensity owing to mass flowrate, which will be explained in Section 3.2. Inside the vortices there are stagnant zones, where huge disparity of velocity exists compared with the main flow. Reason for this difference is the same line arrangement of CC inlet and outlet. As the streamline starts to skew, the fluid velocity near the wick increases, weakening the subcooled flow boiling and reducing the vapor volume inside CC. It is also worth noting that the bubbles are trapped in vortex center, which further amplifies the uneven distribution of the vapor phase. Thus, the flow structure conversion is irreversible.

The variation of fluid temperature and distribution of nucleation sites on wick surface are shown in Fig. 3. The black dots represent the generated bubbles, directly relating to the nucleation sites of subcooled flow boiling. It is apparent that temperature changes not only with time but also with flow structure. The disturbance of the fluid on the right side of the wick surface is higher and the temperature is lower. At 10.1 s an obvious deflection happens on temperature. Explanation for such conversion is the influence by the generation of asymmetrical vortices. Fluid temperature on stagnant zones inside the vortices is 2 K higher than the saturated temperature, which results in the formation of nucleation sites on wick surface and causes the generation of subcooled flow boiling inside the CC. Due to a velocity increase near the wick surface by asymmetrical flow structure, the superheated zones shrink, leading to a reduction on nucleation site density along with time variation.

The velocity field on wick surface is depicted in Fig. 4. It has a forward flow in the center of the wick surface along the main flow direction, and two symmetrical backward flows near the evaporator shell. Reason for this flow behavior is the peculiarity of chamber structure. In addition, the liquid velocity decreases rapidly after it scours right side of the wick surface. At 10.1 s, similar deflection in velocity near the wick caused by asymmetrical vortices can be observed. Fig. 5 presents the flow convection on wick surface at 10.1 s. The convective heat transfer coefficient is calculated by

$$h_c = \frac{Q}{A_w\left(T_w - \frac{T_{cc,in} + T_{cc,out}}{2}\right)} \tag{19}$$

where T_w is the local wick surface temperature, $T_{cc,in}$ and $T_{cc,out}$ are the temperatures at CC inlet and outlet respectively, A_w is the local heat transfer surface area. It performs that the convective heat transfer coefficient has a similar distribution compared with velocity and temperature, and it reaches the maximum at the highest value of velocity. On the left side of the wick surface, a lower velocity results in a reduction in convective heat transfer coefficient. Another noticeable thing is that there are some zones with minimal coefficient, where phase change turns to be the main heat transfer method, causing the formation of stagnant zones and nucleation sites. Adhesion bubbles obstruct the heat transfer from wick to liquid, which further reduces the local convective heat transfer capacity.

3.2. Effect of mass flowrate

The mass flowrate at CC inlet has significant influence on the evaporator performance. In conventional LHP, mass flowrate varies with heat load automatically. When working on a low mass flowrate or high heat load, heat leak can be so high that the saturated boiling will happen inside CC, and this further results in temperature fluctuation or even system failure. However, in pump-assisted LHP, mass flowrate does not alter with heat load, which leads to a smaller temperature fluctuation. In this section two different mass flowrates designated as case 1 and case 3 in Table 2 are investigated, one is 3.75 g/s and the other is 11.25 g/s. The simulation results of these two groups are compared with case 2 in Section 3.1. Fig. 6 displays the variation of fluid temperature and distribution of nucleation sites on wick surface at 10.1 s.

The result illustrates that by changing mass flowrate, the flow structure varies significantly. Compared with Fig. 3(c) when flow time is the same, lower mass flowrate in Fig. 6(a) leads to more nucleation sites dispersing on wick except for a small part that is first scoured by the main flow. But for higher mass flowrate in Fig. 6(b), only a few nucleation sites get formed. Reducing mass flowrate causes a decrease

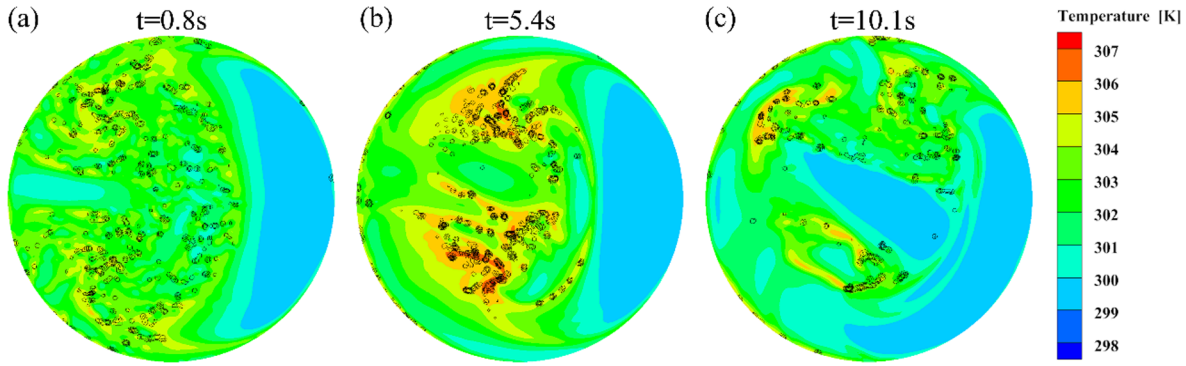

Fig. 3. Fluid temperature and nucleation sites distribution on wick surface: (a) t = 0.8 s; (b) t = 5.4 s; (c) t = 10.1 s.

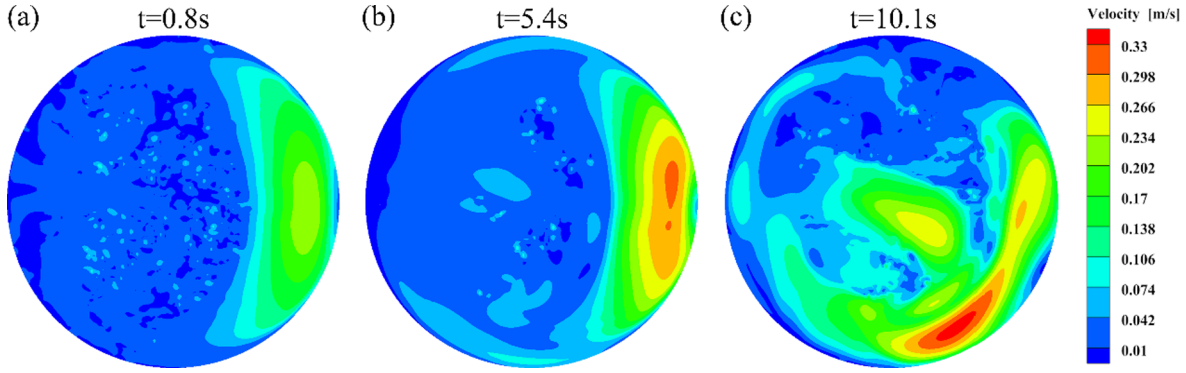

Fig. 4. Velocity field of fluid on wick surface: (a) t = 0.8 s; (b) t = 5.4 s; (c) t = 10.1 s.

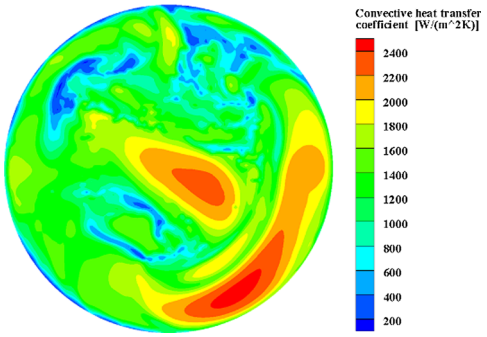

Fig. 5. Convective heat transfer coefficient on wick surface at 10.1 s.

in CC inlet velocity, that in turn declines the velocity on wick surface. Similarly, for the low mass flux in conventional LHP, the low velocity fluid near the wick is insufficient to compensate high heat leak coming from wick and evaporator shell, thus inducing saturated boiling. In that case, intermittent detachment of bubbles can be the main reason for temperature fluctuation. With the assistance of pump, the increase in velocity on wick surface can promote convective heat transfer as well as decrease nucleation sites, thereby suppressing saturated boiling into subcooled flow boiling and reducing temperature fluctuation range. The greater the pump power, the lower the intensity of subcooled flow boiling and the fewer the nucleation sites. The temperature distribution can be a way to reflect fluid behavior, which means that there still keeps symmetric vortices structure at low mass flowrate, but asymmetrical vortices at high mass flowrate. This reveals another factor for the generation of asymmetrical vortices. Increasing mass flowrate results in an augment in turbulence intensity, thus raising the instability of hydrodynamic behaviors. Although there exist tremendous bubbles at 3.75 g/s, vapor distribution on the upper side of chamber is nearly symmetrical. As a result, the effect of vapor on streamline is almost negligible. When mass flowrate accelerates, the turbulence intensity becomes even intensified, the deflection caused by bubbles and flow instability is more pronounced.

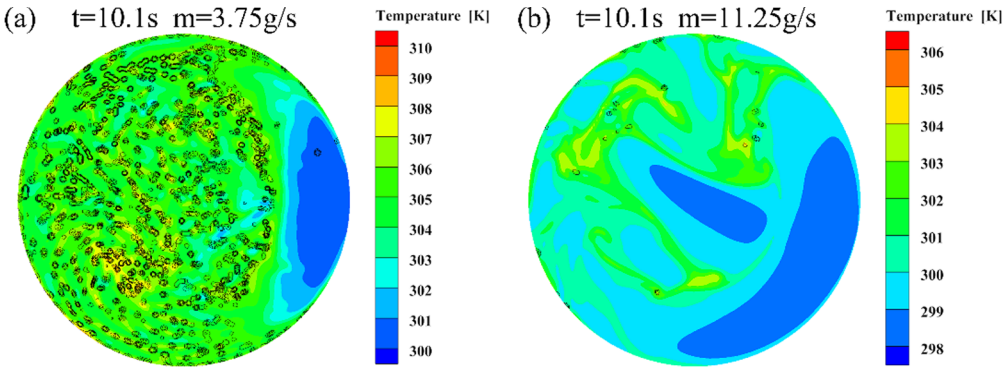

Fig. 6. Fluid temperature and nucleation sites distribution on wick surface: (a) m = 3.75 g/s, t = 10.1 s; (b) m = 11.25 g/s, t = 10.1 s.

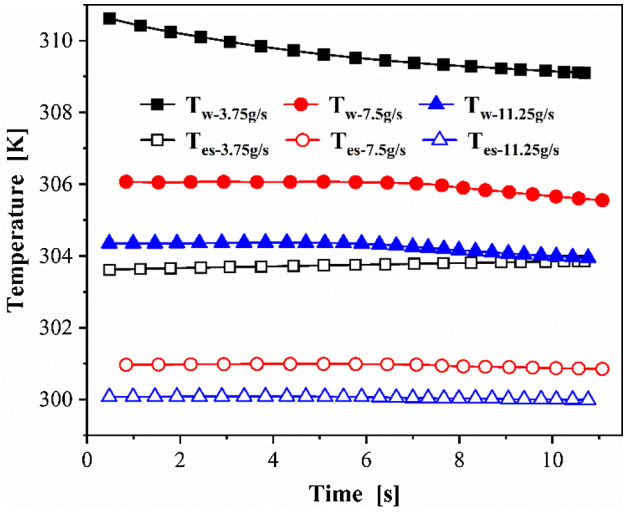

Fig. 7. Average temperature under different mass flowrates.

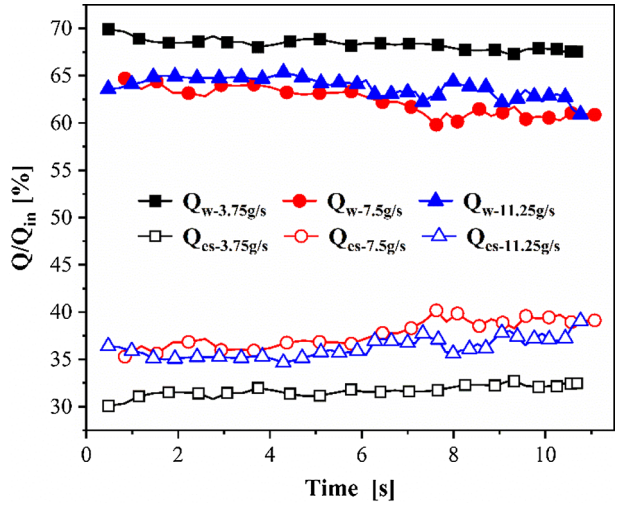

Fig. 8. Surface heat flux under different mass flowrates.

The average temperature at wick surface and evaporator shell internal surface both in contact with fluid under different mass flowrate are displayed in Fig. 7. Subscript *w* and *es* declare wick surface and evaporator shell internal surface respectively (see Fig. 1(b)). Overall, due to the increase in mass flowrate, both temperature on wick surface and evaporator shell internal surface decrease. The wick surface temperatures under three mass flowrates are all higher than saturation temperature, but the deviations are different. When mass flowrate is 3.75 g/s, temperature on wick surface is around 310 K, higher than saturation temperature by 7 K, this results in a nearly saturated boiling on wick surface. For the other two groups, superheat degrees for 7.5 g/s and 11.25 g/s are 3 K and 1 K respectively. Such reduction in superheat degree contributes to a conversion from saturated boiling into subcooled flow boiling as well as an enhancement in convective heat transfer. After 6 s, flow structure shifts into asymmetrical vortices. Therefore, a small decrease in temperature happens on wick surface at 7.5 g/s and 11.25 g/s.

The heat flux into fluid can be divided into two parts, one on wick surface and the other on evaporator shell internal surface (see Fig. 1(b)). Although the contact area between the wick and evaporator shell is small, there is a considerable heat flux through that interface on account of high thermal conductance, resulting in a difference between surface heat flux and boundary condition heat leak. Fig. 8 presents the ratio of surface heat flux to the total value under different mass flowrates. It is obvious that it doesn't always keep the same as 2:1, which is the boundary condition heat leak ratio. Heat flux on wick surface at 3.75 g/s is bigger than the other two groups, but at 7.5 g/s it is slightly lower than that of 11.25 g/s. Such a diversity is the consequence of two different boiling mechanisms. For mass flowrate of 3.75 g/s, a large number of bubbles generate on wick surface, causing a higher intensity of phase change heat transfer than convective heat transfer. This accounts for a larger heat flux on wick surface. When subcooled flow boiling gets formed in CC under larger mass flowrate, heat taken by convection dominates, which indicates that a higher velocity at 11.25 g/s takes much more heat from the wick surface than 7.5 g/s.

3.3. Effect of heat leak

From Fig. 1(b), the simulation separates heat leak into two parts, one from wick and the other from evaporator shell. Changing the total heat leak and heat leak ratio will influence the heat and mass transfer mechanism. Therefore, three different groups of heat leak are carried out (see Table 2). The heat leak of wick and evaporator shell for cases 4–6 are 8 W and 4 W, 12 W and 6 W, 6 W and 12 W respectively.

Fig. 9 presents the fluid temperature and nucleation sites on wick surface at about 10 s. From Figs. 9(a) and 3(c), changing the inlet subcooled fluid temperature while keeping other initial parameters the same, a conclusion can be summarized. Namely, increasing inlet subcooled degree can effectively reduce nucleation sites density by decreasing chamber temperature, thus reducing the intensity of subcooled flow boiling and restraining the transform in flow structure.

Adding heat leak increases nucleation sites significantly (see Fig. 9(a) and (b)). This indicates that even at high subcooled degree, if the heat leak is high enough, the subcooled flow boiling can get formed

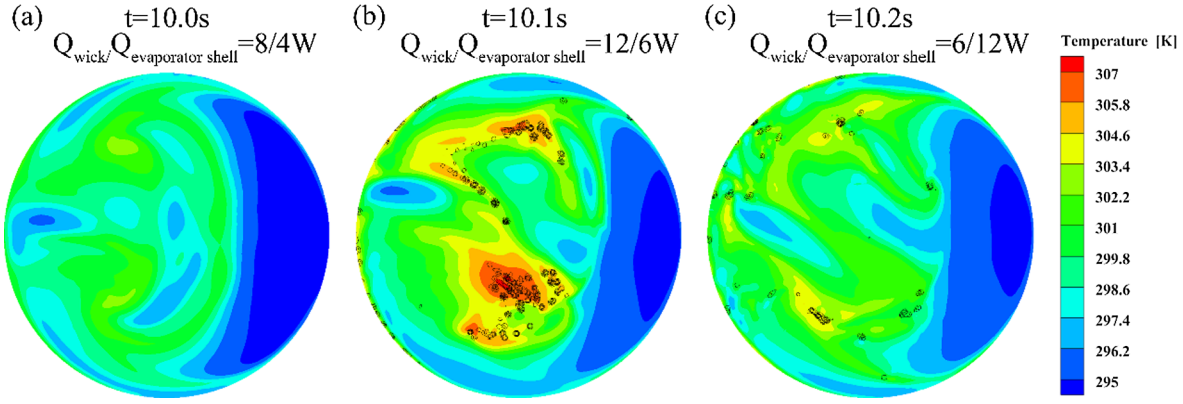

Fig. 9. Fluid temperature and nucleation sites distribution on wick surface: (a) $Q_{wick}/Q_{evaporator\ shell}$ = 8/4 W, t = 10.0 s; (b) $Q_{wick}/Q_{evaporator\ shell}$ = 12/6 W, t = 10.1 s; (c) $Q_{wick}/Q_{evaporator\ shell}$ = 6/12 W, t = 10.2 s.

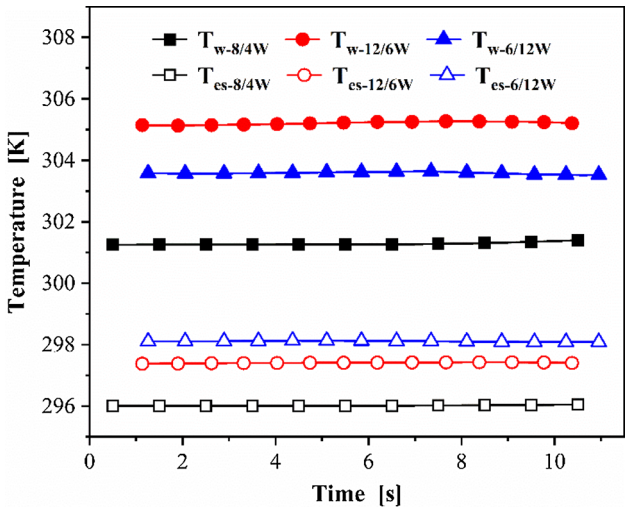

Fig. 10. Average temperature under different heat leaks.

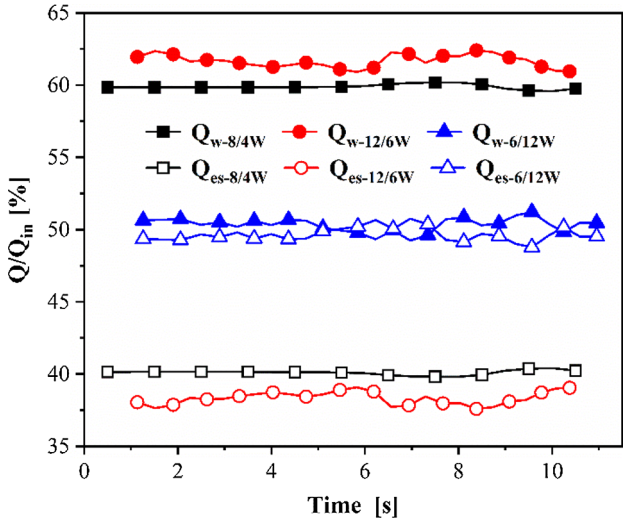

Fig. 11. Surface heat flux under different heat leaks.

as well. Simulation results of heat leak allocations are demonstrated by Fig. 9(b) and (c). Although the wick thermal conductivity is relativity high, heat flux on the middle of the wick is still too hard to be conducted to evaporator shell due to the long heat transfer distance. However, heat flux from the bottom of the evaporator shell can be transferred vertically to the upper side of the chamber where higher velocity fluid scours. As a result, nucleation sites in (b) are more than (c) and superheated zones are also larger and more concentrate on wick surface, indicating that subcooled flow boiling mainly forms on wick surface.

A higher heat leak from evaporator shell can result in temperature tendency different from mass flowrate. Fig. 10 presents average temperature at wick surface and evaporator shell internal surface. The comparison between red and black curves indicates that when the heat leak rises, both average temperature at wick surface and evaporator shell internal surface increase. This causes a 2 K superheat degree, and results in the formation of nucleation sites and subcooled flow boiling. Moreover, as heat leaks vary from 12/6 W to 6/12 W, more heat can be conducted to the upper fluid, thus, a reduction of 1.5 K on wick surface and increment of 0.5 K on evaporator shell internal surface can be explicitly obtained and explained.

Fig. 11 describes the variation of heat flux from two surfaces into fluid. Adding heat leak while keeping ratio the same, heat eliminated from wick surface is increased due to the vaporization of subcooled

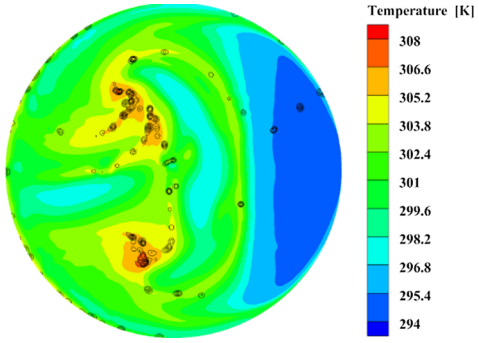

Fig. 12. Fluid temperature and nucleation sites distribution on wick surface when considering environmental convection.

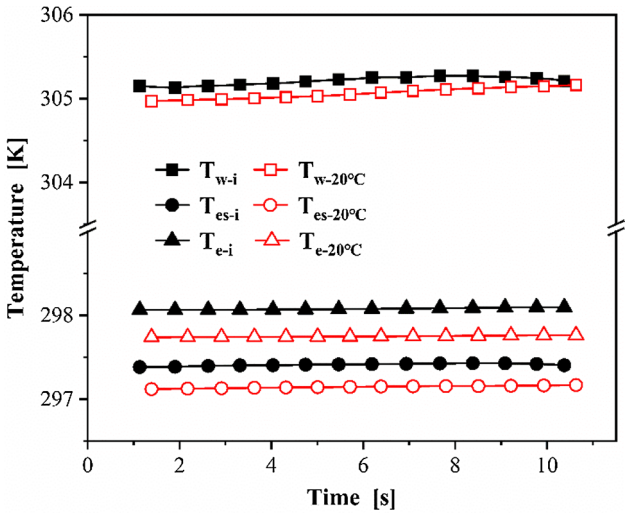

Fig. 13. Environmental influence on average temperature.

flow boiling. Furthermore, the fluctuation of heat flux is intensified contrast to single phase convection heat transfer. Even though it is a porous media, the effective thermal conductivity of the wick is still higher than evaporator shell, which leads a part of heat to flow towards wick when evaporator shell heat leak is higher. Thus, altering heat leaks from 12/6 W to 6/12 W, the heat fluxes at two internal surfaces convert to nearly the same.

3.4. Effect of environmental convection

In experimental studies and realistic applications, the evaporator of LHP is not insulated from the ambient. By setting convective heat transfer coefficient to 50 W/(m^2·K) (air forced convection) and environment temperature to 20 °C while keeping other boundary parameters the same as case 5, the effect of the ambient can be evaluated.

Comparing Figs. 12 and 9(b), a slight shrink in superheated zones and a decrease of nucleation sites are observed. The environmental convection offers a new path for dissipating heat leak, then induces a decline of heat flux on wick surface. Another noticeable thing is that the temperature distribution is different, indicating a difference on the offset direction of streamline, which can be explained by the flow instability due to the randomness of vapor distribution.

Taking environmental heat loss into account under constant heat leak can decrease the heat absorbed by fluid. Fig. 13 presents average temperature on three surfaces, two of which have been stated in Section 3.1. Subscript *e* declares outer surface of the evaporator shell which is exposed to the ambient (see Fig. 1(b)). Subscript *i* (adiabatic) declares the condition without environmental heat loss, and subscript 20 °C is

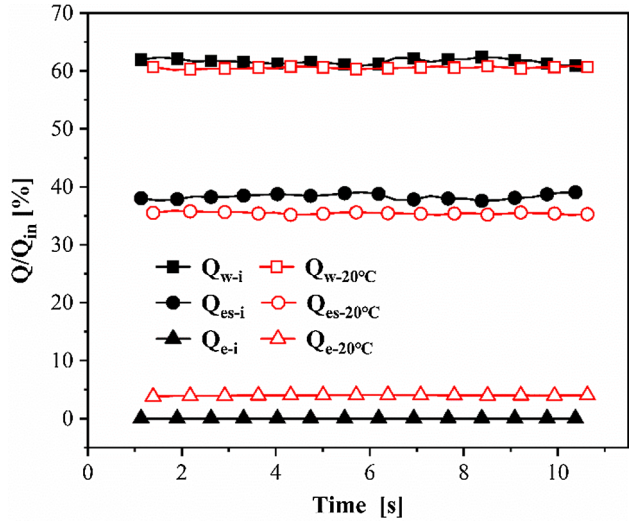

Fig. 14. Environmental influence on surface heat flux.

the opposite. It demonstrates that heat flux to environment can reduce the temperature of each part inside CC, but the deviations are not the same. Heat leak on the middle of the wick surface is hard to be transferred to the ambient, thus resulting in a smaller reduction on wick surface than evaporator shell internal surface. Heat flux variation on three surfaces is displayed in Fig. 14. A visible discrepancy can be observed that the decrease in evaporator shell internal surface heat flux is larger than wick surface when adding environmental convection. Besides, 4% of the heat leak dissipates to the ambient, indicating that the environment has trivial impact on heat and mass transfer in CC even under air forced convection. Here the evaporator shell only includes CC side, heat flux to the ambient may increase when the remaining part at vapor chamber side is considered.

4. Conclusion

A three-dimensional CFD model has been developed to simulate the thermal-hydrodynamic behavior in compensation chamber of a pump-assisted loop heat pipe. By using the VOF method, the phase change in compensation chamber under high heat leak is fully considered. The effects of mass flowrate, heat leak distribution, and environmental convection have been investigated in detail. The main conclusions are as follows:

(1) Simulation results demonstrate that subcooled flow boiling happens inside compensation chamber, and the gas–liquid two-phase flow is the main reason for the temperature fluctuation on CC outlet. Due to the uneven vapor distribution and turbulence intensification, the flow structure converts, which leads to a shrink in stagnant zones and reduction on subcooled flow boiling intensity.
(2) Low mass flowrate in conventional LHP results in a saturated boiling rather than subcooled flow boiling. The intermittent detachment of bubbles can be the main reason for larger temperature fluctuation. Increasing mass flowrate can raise the turbulence intensity and promote the flow structure transformation, thus the wick temperature and nucleation site density can be reduced.
(3) Subcooled flow boiling can be generated even at high subcooled degree when total heat leak increases, and the surface heat flux is found to be significantly affected by the heat leak ratio variation. Specifically, the intensity of subcooled flow boiling can be enhanced when heat leak from wick is dominant.
(4) Environmental convection does slight effect on subcooled flow boiling for the heat leak to the ambient is less than 5%. Meanwhile, the effect of environmental heat loss on evaporator shell is more obvious as compared with wick due to a closer thermal transfer path.

Declaration of Competing Interest

The authors declared that there is no conflict of interest.

Acknowledgement

This work was supported by the National Natural Science Foundation of China (No. 51736004 and No. 51776079).

References

[1] Y.F. Maydanik, Loop heat pipes, Appl. Therm. Eng. 25 (2005) 635–657.
[2] P.M. Dussinger, D.B. Sarraf, W.G. Anderson, Loop Heat Pipe for TacSat-4, in: AIP Conference Proceedings, Vol. 1103, AIP, 2009, pp. 91-100.
[3] Y.F. Maydanik, S.V. Vershinin, V.G. Pastukhov, S. Fried, Loop heat pipes for cooling systems of servers, IEEE Trans. Compon. Packag. Technol. 33 (2010) 416–423.
[4] X. Lu, T. Hua, M. Liu, Y. Cheng, Thermal analysis of loop heat pipe used for high-power LED, Thermochim Acta 493 (2009) 25–29.
[5] R. Singh, A. Akbarzadeh, C. Dixon, M. Mochizuki, Novel design of a miniature loop heat pipe evaporator for electronic cooling, J. Heat Transfer 129 (2007) 1445–1452.
[6] R. Singh, A. Akbarzadeh, M. Mochizuki, Effect of wick characteristics on the thermal performance of the miniature loop heat pipe, J. Heat Transfer 131 (2009) 082601.
[7] J. Esarte, J. Blanco, A. Bernardini, J. San-José, Optimizing the design of a two-phase cooling system loop heat pipe: Wick manufacturing with the 3D selective laser melting printing technique and prototype testing, Appl. Therm. Eng. 111 (2017) 407–419.
[8] B. Siedel, V. Sartre, F. Lefevre, Complete analytical model of a loop heat pipe with a flat evaporator, Int. J. Therm. Sci. 89 (2015) 372–386.
[9] B. Siedel, V. Sartre, F. Lefèvre, Numerical investigation of the thermohydraulic behaviour of a complete loop heat pipe, Appl. Therm. Eng. 61 (2013) 541–553.
[10] V.V. Vlassov, R.R. Riehl, Mathematical model of a loop heat pipe with cylindrical evaporator and integrated reservoir, Appl. Therm. Eng. 28 (2008) 942–954.
[11] L. Bai, G. Lin, H. Zhang, D. Wen, Mathematical modeling of steady-state operation of a loop heat pipe, Appl. Therm. Eng. 29 (2009) 2643–2654.
[12] L. Bai, G. Lin, D. Wen, Modeling and analysis of startup of a loop heat pipe, Appl. Therm. Eng. 30 (2010) 2778–2787.
[13] M.A. Chernysheva, Y.F. Maydanik, Numerical simulation of transient heat and mass transfer in a cylindrical evaporator of a loop heat pipe, Int. J. Heat Mass Transf. 51 (2008) 4204–4215.
[14] M. Nishikawara, H. Nagano, T. Kaya, Transient thermo-fluid modeling of loop heat pipes and experimental validation, J. Thermophys Heat Transfer 27 (2013) 641–647.
[15] M. Lee, C. Park, Mechanical-capillary-driven two-phase loop: Numerical modeling and experimental validation, Int. J. Heat Mass Transf. 125 (2018) 972–982.
[16] J. Li, G.P. Peterson, 3D heat transfer analysis in a loop heat pipe evaporator with a fully saturated wick, Int. J. Heat Mass Transf. 54 (2011) 564–574.
[17] M. Ghajar, J. Darabi, N. Crews, A hybrid CFD-mathematical model for simulation of a MEMS loop heat pipe for electronics cooling applications, J. Micromech. Microeng. 15 (2005) 313–321.
[18] M. Ghajar, J. Darabi, Numerical modeling of evaporator surface temperature of a micro loop heat pipe at steady-state condition, J. Micromech. Microeng. 15 (2005) 1963–1971.
[19] M.A. Chernysheva, Y.F. Maydanik, 3D-model for heat and mass transfer simulation in flat evaporator of copper-water loop heat pipe, Appl. Therm. Eng. 33–34 (2012) 124–134.
[20] K. Zhao, Q. Li, Y. Xuan, Investigation on the three-dimensional multiphase conjugate conduction problem inside porous wick with the lattice Boltzmann method, Sci. China Ser. E: Technol. Sci. 52 (2009) 2973–2980.
[21] Q. Li, K. Zhao, Y. Xuan, Simulation of flow and heat transfer with evaporation in a porous wick of a CPL evaporator on pore scale by lattice Boltzmann method, Int. J. Heat Mass Transf. 54 (2011) 2890–2901.
[22] M. Nishikawara, H. Nagano, M. Prat, Numerical study on heat-transfer characteristics of loop heat pipe evaporator using three-dimensional pore network model, Appl. Therm. Eng. 126 (2017) 1098–1106.
[23] A.A. Pozhilov, D.K. Zaitsev, E.M. Smirnov, A.A. Smirnovsky, Numerical simulation of heat and mass transfer in a 3D model of a loop heat pipe evaporator, St. Petersburg Polytech. Univ. J. Phys. Math. 3 (2017) 210–217.
[24] J. Ku, Operating characteristics of loop heat pipes, in, SAE Technical Paper, No. 1999-01-2007, 1999.
[25] K.-H. Cheung, T.T. Hoang, J. Ku, T. Kaya, Thermal performance and operational characteristics of loop heat pipe (NRL LHP), in, SAE Technical Paper, No. 981813, 1998.
[26] D. Wang, Z. Liu, J. Shen, C. Jiang, B. Chen, J. Yang, Z. Tu, W. Liu, Experimental study of the loop heat pipe with a flat disk-shaped evaporator, Exp. Therm Fluid Sci. 57 (2014) 157–164.
[27] X. Zhang, J. Huo, S. Wang, Experimental investigation on temperature oscillation in

a miniature loop heat pipe with flat evaporator, Exp. Therm Fluid Sci. 37 (2012) 29–36.
[28] M.A. Chernysheva, V.G. Pastukhov, Y.F. Maydanik, Analysis of heat exchange in the compensation chamber of a loop heat pipe, Energy 55 (2013) 253–262.
[29] A. Anand, A. Jaiswal, A. Ambirajan, P. Dutta, Experimental studies on a miniature loop heat pipe with flat evaporator with various working fluids, Appl. Therm. Eng. 144 (2018) 495–503.
[30] G. Spinato, N. Borhani, B.P. d'Entremont, J.R. Thome, Time-strip visualization and thermo-hydrodynamics in a closed loop pulsating heat pipe, Appl. Therm. Eng. 78 (2015) 364–372.
[31] C. Jiang, W. Liu, Z. Liu, J. Yang, B. Duan, X. Luo, Startup characteristics of pump-assisted capillary phase change loop, Appl. Therm. Eng. 126 (2017) 1115–1125.
[32] C. Jiang, W. Liu, H.C. Wang, D.D. Wang, J.G. Yang, J.Y. Li, Z.C. Liu, Experimental investigation of pump-assisted capillary phase change loop, Appl. Therm. Eng. 71 (2014) 581–588.
[33] C. Jiang, Z. Liu, D. Wang, J. Yang, H. Wang, J. Li, W. Liu, Effect of liquid charging process on the operational characteristics of pump-assisted capillary phase change loop, Appl. Therm. Eng. 91 (2015) 953–962.
[34] C.W. Hirt, B.D. Nichols, Volume of fluid (VOF) method for the dynamics of free boundaries, J. Comput. Phys. 39 (1981) 201–225.
[35] R. Zhuan, W. Wang, Simulation on nucleate boiling in micro-channel, Int. J. Heat Mass Transf. 53 (2010) 502–512.
[36] Z. Liu, B. Sunden, J. Yuan, Numerical Modelling of Condensation of Multiple Bubbles in Subcooled Flow Boiling With VOF Method, in: ASME 2013 Heat Transfer Summer Conference collocated with the ASME 2013 7th International Conference on Energy Sustainability and the ASME 2013 11th International Conference on Fuel Cell Science, Engineering and Technology. American Society of Mechanical Engineers, V001T03A014, 2013.
[37] H. Jouhara, B. Fadhl, L.C. Wrobel, Three-dimensional CFD simulation of geyser boiling in a two-phase closed thermosyphon, Int. J. Hydrogen Energy 41 (2016) 16463–16476.
[38] Z. Lin, S. Wang, R. Shirakashi, L. Winston Zhang, Simulation of a miniature oscillating heat pipe in bottom heating mode using CFD with unsteady modeling, Int. J. Heat Mass Transf. 57 (2013) 642–656.
[39] J.U. Brackbill, D.B. Kothe, C. Zemach, A continuum method for modeling surface tension, J. Comput. Phys., 100 (1992) 335-354 %@ 0021-9991.
[40] C. Jiang, Performance Investigation and System Simulation of Pump-assisted Capillary Phase Change Loop, (PhD dissertation), Huazhong University of Science and Technology, Wuhan, P.R.China, 2017.